NANO, MESO, MICRO : SCIENCES ET INNOVATIONS POUR LA RADIO ET LA PHOTONIQUE.

Analyse circuit équivalent d'un absorbant radar à métasurface
Equivalent circuit analysis of a radar absorbing metasurface

Tanguy Lopez[1,2], Thomas Lepetit[1], Shah Nawaz Burokur[2]
[1]DEMR, ONERA, Université de Paris-Saclay, F91123 Palaiseau, France
[2]LEME, UPL, Univ Paris Nanterre, F92410 Ville d'Avray, France
tanguy.lopez@onera.fr / tlopez@parisnanterre.fr

Mots clés: métasurface, absorbant radar, circuit équivalent
Keywords : metasurface, radar absorber, equivalent circuit

Résumé/Abstract

Pour toujours plus de camouflage, les experts en furtivité envisagent depuis quelques temps d'utiliser les métasurfaces et leurs propriétés non-conventionnelles de manipulation des ondes [1] pour réaliser des solutions de dissimulation efficaces. En prévision de l'ajout de composants électroniques, permettant notamment de piloter la fréquence pour laquelle le besoin de furtivité se fait ressentir, nous nous sommes intéressés à une approche circuit équivalent pour la conception de métasurfaces. En effet, les travaux de [2] proposent d'analyser des métasurfaces avec électronique en combinant le comportement de la structure d'accueil à celui des composants individuels. L'analyse circuit équivalent de la métasurface d'accueil dénuée de composants peut se faire grâce aux travaux synthétisés dans [3]. Ce projet consiste donc à transposer les résultats de [3] vers la géométrie coaxiale d'intérêt ici. La validité de la méthode est alors éprouvée par comparaison à des résultats de simulation par éléments finis.

To provide for an ever-increasing need for camouflage, experts in stealth have been envisioning for a few years to use metasurfaces and their unconventional electromagnetic properties [1] to serve as efficient cloaking devices. To prepare for the use of surface-mounted electronic components, useful for frequency-selecting purposes, we took interest in an equivalent circuit analysis of metasurfaces. Indeed, the works of [2] on metasurfaces using electronic components invite one to combine the passive behavior of the host structure with that of the lumped elements. The equivalent circuit analysis of the hosting surface deprived of electronic components can be done using the works of [3] on passive metasurfaces. This project therefore aims at translating the results of [3] onto the coaxial geometry of interest here. The validity of such a method is then assessed by comparison with the simulation results obtained using a finite-element method.

1 Introduction

Metasurfaces are arrays of sub-wavelength patterns used in all electromagnetic domains – from optics to microwaves – to design devices with extraordinary wave manipulation properties [1]. Thanks to the Floquet theory [4], the analysis of periodic structures can be simplified down to the study of a single of their constituting metacell. The study of isolated metacells can be conducted under many forms – using a method of moments or finite-element methods for instance. Here, the chosen method is an equivalent circuit analysis (ECA) which would provide the operator with an intelligible equivalent circuit model (ECM) of metacells easily affected by the addition of series and/or parallel impedances of surface-mounted electronic components, as intended in future works.

In [3], an ECA is introduced in the case of metasurfaces studied in free-space and simplified to Cartesian metacells, seen as discontinuities in rectangular waveguides with periodic boundaries. In this project, this method is applied to a metacell in a coaxial geometry – this translation is possible as the method proposed in [3] is independent of the chosen system of coordinates. This coaxial geometry is chosen to accelerate the design cycle by reducing fabrication costs, along with measurement complexity. In addition, such coaxial geometry emulates free-space propagation by supporting a TEM propagation mode, and therefore allows for measurements at low frequencies in a compact setup.

In the frame of this project, the studied metacell is that of Figure 1(a) – a PCB of coaxial geometry into which eight identical apertures have been cut out. The metacell of Figure 1(a) is then inserted into a coaxial transmission line (TL) terminated by a short-circuit as illustrated on Figure 1(b). In such configuration, the short-circuit is a stand-in for the target's fuselage or external metallic structure.

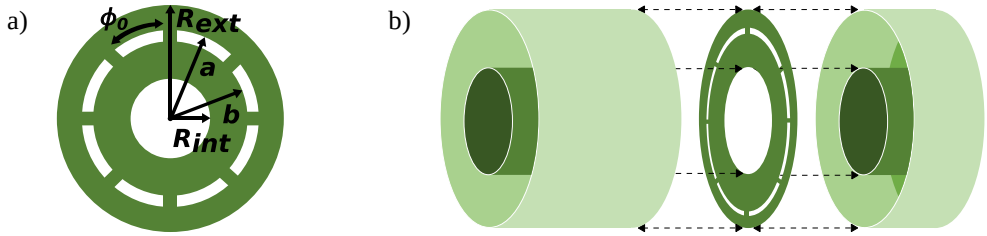

Figure 1: (a) Metacell of interest with its eight identical apertures with R_{ext} = 75 mm, R_{int} = 32.5 mm, a = 56.25 mm, b = 51.25 mm and $\phi_0 = \pi/4$ and (b) the coaxial TL used for this study is terminated by a short-circuit

Knowledge of the dimensions of the coaxial TL of Figure 1(b) allows one to locate the exact cut-off frequencies, from which the higher-order TE and TM modes turn propagative, thanks to the Bessel-Neumann's equations [5] and their numerical implementation [6]. This leads to the values reported on Figure 2 for the first modes of interest – truncated for legibility. This information is key for the application of the method of [3], whose equivalent circuit depends on the couplings of the metasurface's electric field to the surrounding TL modes.

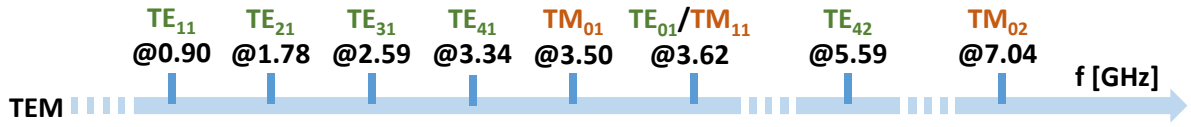

Figure 2: Cut-off frequencies of the TE_{nm} and TM_{nm} propagation modes of interest supported in the coaxial TL

2 Equivalent circuit analysis

2.1 General study in a coaxial transmission line

The ECA proposed by [3] is an attempt at reaching an analytical expression of the metacell's admittance Y_{MS} encountered by the incoming wave of admittance Y_0 propagating within the TL as presented on Figure 3.

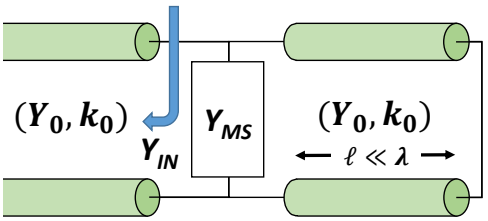

Figure 3: General equivalent circuit model of a metacell introduced in a short-circuited TL

In such configuration, the reflection coefficient of the network formed by the metacell introduced in the short-circuited TL is given by

$$S_{11} = \frac{Y_0 - Y_{IN}}{Y_0 + Y_{IN}} \qquad (1)$$

The ECA introduced in [3] is able to provide an analytical expression of such a reflection coefficient provided prior knowledge of two elements: a decomposition basis and an expression of the metacell's electric field $\boldsymbol{E_S}$. The first element is provided by the modal basis of coaxial fields $\boldsymbol{e_{nm}}$, normalized according to [5]. The second element however urges one to express a fundamental two-part work hypothesis. Firstly, that the total electric field of the metacell $\boldsymbol{E_S}$ is the superposition of the fields supported by each of the apertures. Secondly, that the field supported by each of these apertures is the fundamental mode supported by the equivalent waveguide. In the case of this project, the metacell's electric field $\boldsymbol{E_S}$ is therefore seen as the superposition of the fields of eight identical apertures seen as the cross-sections of finite-arc-lengthed coaxial waveguides, called *double-baffled coaxial waveguides* in [7] where an analytical expression of the various modes supported by such a waveguide is provided.

Once these expressions are found, the electric field $\boldsymbol{E_S}$ of the metacell may be expressed in the modal basis using the projections N_{nm} introduced in [3] and defined as

$$N_{nm} = \langle \boldsymbol{E_s} | \boldsymbol{e_{nm}} \rangle = \int_S \boldsymbol{E_s} . \boldsymbol{e_{nm}^*} dS \qquad (2)$$

Which are particularly convenient for building an ECM as in the specific case where the frequency and spatial dependencies of the metacell's $\boldsymbol{E_S}$ field are separable, the N_{nm} projections can be seen as transformer ratios.

According to [3] and the modal basis decomposition of [5], it is possible to separate each harmonic supported by the coaxial TL into individual TLs propagating each a modal coaxial wave admittance Y_{nm}. Given the configuration of the coaxial TL of Figure 1(b), the TL theory claims [8] that such admittances are seen by the metacell as: either unaffected – as fed by the infinite TL on one side – or affected by the short-circuit found at a distance $\ell \ll \lambda$ on the other side. For the study in reflection of the incident TEM coaxial mode, the remaining TE_{nm} and TM_{nm} coaxial modes' local interactions with the metacell thus introduce a perturbation in the form of an equivalent admittance Y_{eq} such that

$$Y_{eq} = \sum_{nm \neq inc} |N_{nm}|^2 (1 - jcotan(\beta_{nm}\ell)) Y_{nm} \tag{3}$$

where one may notice the projections N_{nm} of the metacell's field over the modal vectors $\boldsymbol{e_{nm}}$ along with the inductive behavior introduced by the short-circuit in the form of the imaginary part of the formula. Such equivalent admittance implies that an infinite number of harmonics must be explicitly taken into account to provide an accurate ECM. Fortunately, some simplifications can alleviate the weight of such computation.

Indeed, when conducting the study over a frequency range over which some of the supported modes are strongly evanescent *i.e.*, for which $k_{nm} \gg k$, then the admittances of the coaxial TE and TM modes may be simplified to

$$\begin{cases} Y_{nm}^{TM} = \dfrac{1}{\eta_0}\dfrac{k_0}{\beta_{nm}^{TM}} \approx \dfrac{1}{\eta_0}\dfrac{k_0}{-j|k_{nm}^{TM}|} = j\omega C_{nm} \\ Y_{nm}^{TE} = \dfrac{1}{\eta_0}\dfrac{\beta_{nm}^{TE}}{k_0} \approx \dfrac{1}{\eta_0}\dfrac{-j|k_{nm}^{TE}|}{k_0} = \dfrac{1}{j\omega L_{nm}} \end{cases} \tag{4}$$

The implications of Equation (4) are that individual higher-order evanescent modes can be simplified down to a single capacitance, in the case of TM modes, and a single inductance, in the case of TE modes. Splitting up the sum in Equation (3) into TM and TE modes and splitting each of these sums into (n_{prop}^{TM} TM and n_{prop}^{TE} TE) propagative and evanescent modes, the equivalent admittance can be written

$$Y_{eq} = \sum_{n,m}^{n_{prop}^{TM}} |N_{nm}^{TM}|^2 \left(1 - jcotan(\beta_{nm}^{TM}\ell)\right) Y_{nm}^{TM} + \sum_{n,m}^{n_{prop}^{TE}} |N_{nm}^{TE}|^2 \left(1 - jcotan(\beta_{nm}^{TE}\ell)\right) Y_{nm}^{TE} + j\omega C_{ho} + \frac{1}{j\omega L_{ho}} \tag{5}$$

where C_{ho} and L_{ho} are the overall capacitance and inductance introduced by the evanescent TM and TE modes, respectively.

2.2 Particular case of the studied metacell

The fundamental assumption previously made that the eight identical apertures of Figure 1(a) take equal part in the total electric field of the metacell $\boldsymbol{E_S}$ implies that knowing the field of one aperture is enough to know the field of the whole metacell. Using the information given in [7], one may therefore express the electric field of the different modes found within a single aperture of finite arc-length ϕ_0 (see Figure 1(a)). The first thing to acknowledge here is the lack of a TEM mode in such *double-baffled coaxial waveguide*. The fundamental propagation mode of such waveguide must therefore be determined from the cut-off frequencies of the various supported modes.

According to [7], a *double-baffled coaxial waveguide* supports both TE and TM propagations. In the case of TE propagation in such finite-arc-lengthed aperture, the electric field $\boldsymbol{E_{pq}^{TE}}$ with $(p,q) \in \frac{\pi}{\phi_0}\mathbb{N}^* \times \mathbb{N}$ can be expressed in polar coordinates as

$$\boldsymbol{E_{pq}^{TE}}(\rho,\phi) = A \begin{pmatrix} \dfrac{p}{\epsilon\rho}\left(Y_{pq}(k_{pq}\rho) - \alpha'_{pq}J_{pq}(k_{pq}\rho)\right)\sin(p\phi) \\ \dfrac{k_{pq}}{\epsilon}\left(Y'_{pq}(k_{pq}\rho) - \alpha'_{pq}J'_{pq}(k_{pq}\rho)\right)\cos(p\phi) \\ 0 \end{pmatrix} \tag{6}$$

where A is an amplitude constant, J and Y are the Bessel functions of first and second order while J' and Y' are their derivatives regarding the variable ρ, k_{pq} are the cut-off wavenumbers of the considered modes and α'_{pq} a constant that fulfills the boundary conditions of the perfect electric nature of the aperture's rims. One may notice that for $\phi_0 = \pi/4$, then $p = 4n,\ n \in \mathbb{N}^*$, which is the case here (see Figure 1(a)). Using Bessel-Neumann's equations adapted to the case of such *double-baffled coaxial waveguide* according to [7], the cut-off frequencies of the first TM and TE modes of interest have been calculated [6] and the results are reported in Figure 4 for comparison purposes – between each other and regarding the coaxial TL's.

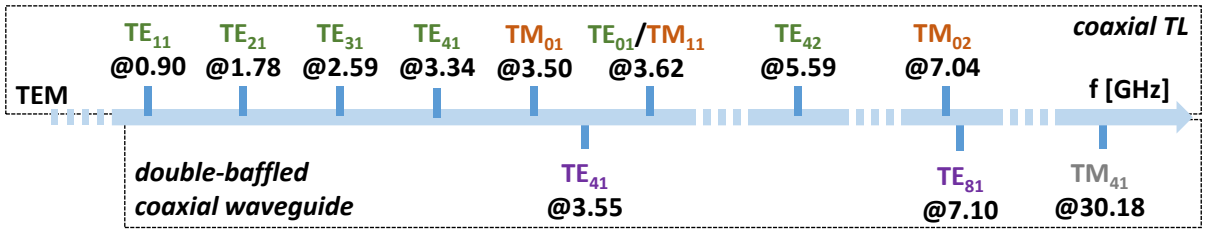

Figure 4: Cut-off frequencies of the TE_{nm} and TM_{nm} modes of the coaxial TL (top) along with the cut-off frequencies of the first TE_{nm} and TM_{nm} modes of the double-baffled coaxial waveguide (bottom)

From Figure 4, the fundamental mode of the single double-baffled waveguide is TE_{41}. The total metacell's electric field $\boldsymbol{E_S}$ as required in Equation (2) is therefore assumed to be

$$\boldsymbol{E_S}(\rho,\phi) = \sum_{k=0}^{7}\left(\boldsymbol{E_{41}^{TE}}\left(\rho,\phi - k\frac{\pi}{4}\right).\Pi_{\pi/4}\left(\phi - (2k+1)\frac{\pi}{8}\right)\right) \qquad (7)$$

where Π_w is the rectangle function of width w – here of width $\phi_0 = \pi/4$ and centered over each aperture.

Finite-element simulations have been performed on a single metacell's aperture from Figure 1(a) (extending in the ranges $\rho \in [a, b]$ and $\phi \in [0, \pi/4]$) and have confirmed the theoretical expression found in Equation (6), as can be seen on Figure 5.

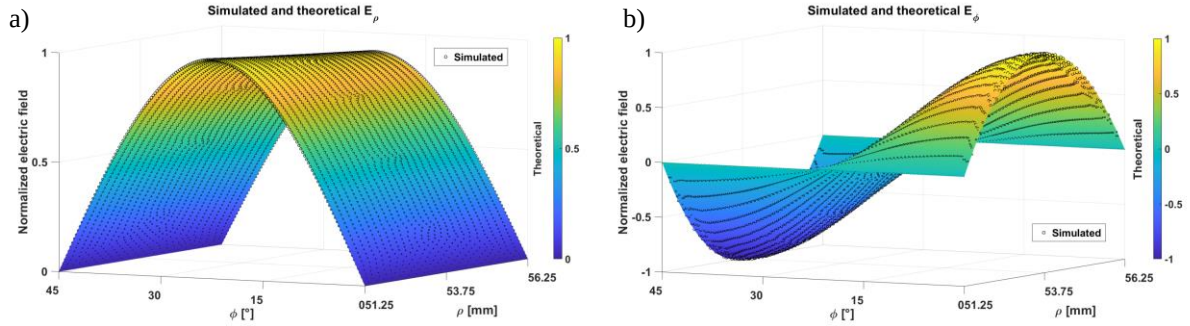

Figure 5: Comparison of the electric field profiles of the fundamental mode of a double-baffled coaxial waveguide for the (a) ρ-component and (b) ϕ-component as provided by COMSOL® (black circles) and Equation (6) (colormap)

The analysis of the projections N_{nm} as defined in Equation (2) quickly highlights that only some of the coaxial TL modes are in fact able to couple with the metacell's electric field $\boldsymbol{E_S}$ from Equation (7). In the case of the simplification $\phi_0 = \pi/4$, some symmetry considerations lead to the results highlighted on Figure 6. The first take is that fortunately, the incident TEM mode can indeed couple with the metacell. The second take is that only the $TE_{4n,m}$, and TM_{0m} modes are to be considered in the equivalent admittance Y_{eq} of Equation (3).

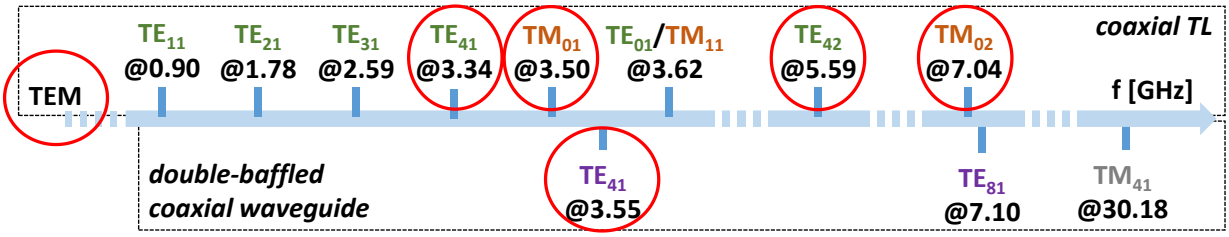

Figure 6: Highlight of the first coaxial TL's $TE_{4n,m}$ and TM_{0m} modes (top) able to couple with the double-baffled coaxial waveguide's fundamental mode (bottom)

2.3 Equivalent circuit model

According to the highlighted coupling modes of Figure 6, the metacell's reflective behavior is only altered by the admittances of the $TE_{4n,m}$, and TM_{0m} modes. Therefore, to observe an alteration of the metacell's reflection coefficient, one can focus on the sole frequency range around the cut-off frequencies of such modes. In other words, over any frequency range below $f_{41}^{TE} \approx 3.34$ GHz (see Figure 6), no noticeable change in the reflection coefficient should be observed.

A closer look at the different transitions exhibited by TE and TM modes around their cut-off frequencies is given on Figure 7. One may notice the coaxial TM_{01} mode exhibits a strongly resonant behavior around its cut-off frequency $f_{01}^{TM} \approx 3.50$ GHz (see Figure 6) – transitioning sharply from a capacitive admittance to a resistive one – while the TE_{41} mode shows a smooth transition from an inductive behavior to a resistive one around f_{41}^{TE}.

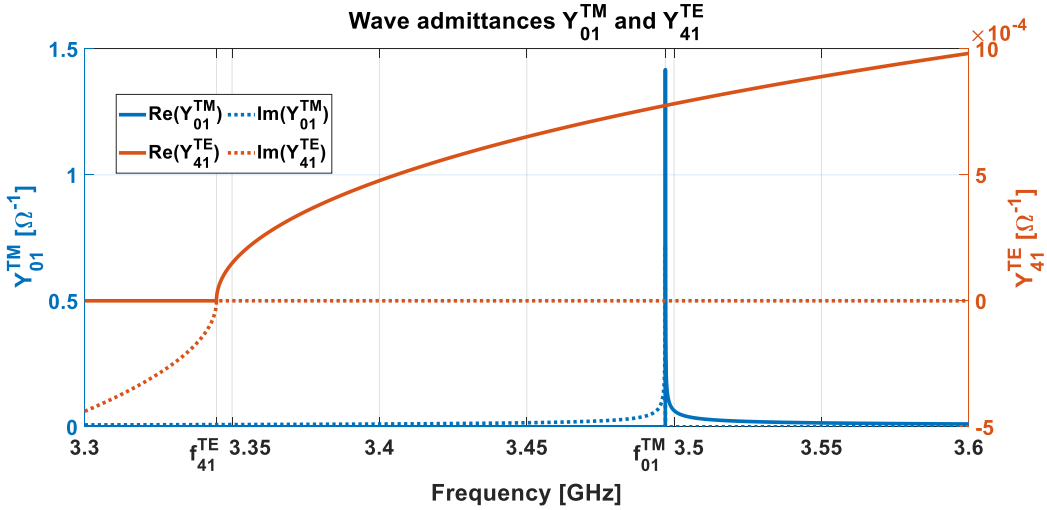

Figure 7: Comparison of wave admittances Y_{01}^{TM} (left axis, blue curves) and Y_{41}^{TE} (right axis, red curves) around their respective cut-off frequency $f_{01}^{TM} \approx 3.50$GHz and $f_{41}^{TE} \approx 3.34$ GHz

Subsequent finite-element simulations highlighted the strong conditioning of the metacell's resonance to the TM transitioning rather than the TE transitioning. This may find an explanation in the definition of the reflection coefficient from Equation (1) : to match the incoming TEM wave of real admittance Y_0, the metacell's admittance Y_{MS} must provide both a resistive part, and a reactive part able to compensate for the inductive behavior induced by the short-circuit. To do so, such reactance must be capacitive, as is provided by the couplings with TM modes, unlike the TE modes whose couplings only add more inductive contributions. The frequency range [3.45, 3.60] GHz around the cut-off frequency of the TM_{01} mode $f_{01}^{TM} \approx 3.50$ GHz has therefore been chosen as a range of interest to assess the ability of the ECM to translate the expected behavior observed by finite-element simulations.

Around the first TM_{01} mode, both the TM_{01} and TE_{41} modes are propagative. According to the equivalent admittance expression from Equation (5), only these two modes are to be explicitly considered in the ECA while the higher-order modes $TM_{0m,m>1}$ and $TE_{4m,m>1}$ are lumped into an equivalent parallel capacitance C_{ho} and inductance L_{ho}, respectively. This leads to the equivalent circuit of Figure 8, which is valid as long as only these modes are propagative *i.e.*, up until the next interacting mode of cut-off frequency $f_{42}^{TE} \approx 5.59$ GHz (see Figure 6).

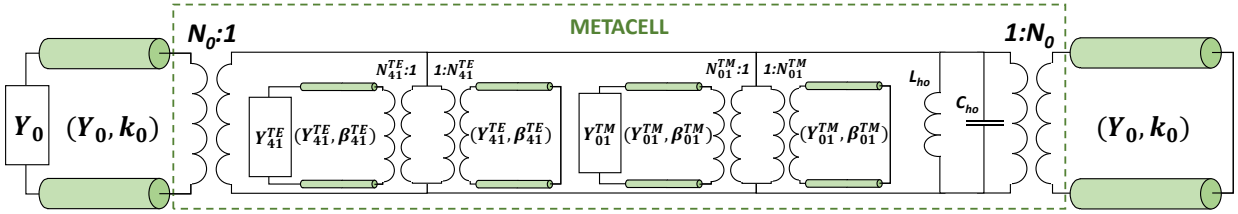

Figure 8: Equivalent circuit model of the metacell introduced in the coaxial TL valid up until 5.59 GHz ($\approx f_{42}^{TE}$)

3 Results

According to Equation (1) and given the ECM of Figure 8, the reflection coefficient is given by

$$S_{11} = \frac{|N_0|^2 Y_0 - \left(-jcotan(k_0 \ell)|N_0|^2 Y_0 + Y_{eq}\right)}{|N_0|^2 Y_0 + \left(-jcotan(k_0 \ell)|N_0|^2 Y_0 + Y_{eq}\right)} \tag{8}$$

The frequency response of such ECM is compared to the reflection coefficient provided by finite-element simulations on Figure 1(b), in terms of both amplitude and phase. One may notice on Figure 9 an amplitude drop along with a phase zero for both curves, which are symptomatic of a resonant behavior: the injected TEM mode sees its power partially transferred to the higher-order modes shown in the ECM of Figure 8 right around the resonance frequency and its power is therefore only partially recovered after reflection.

One may notice on Figure 9 a general shift of the S_{11}-parameter curves provided by the ECM of around 14 MHz which represents a relative shift of around δf_ϕ = 0.4 %. The reflection minimum from Figure 9 has also been shifted by around 34 MHz which represents a δf_A = 1 % downward shift. One may finally notice that the equivalent circuit model has not been able to translate the spectral spreading the finite-element method has highlighted on Figure 9.

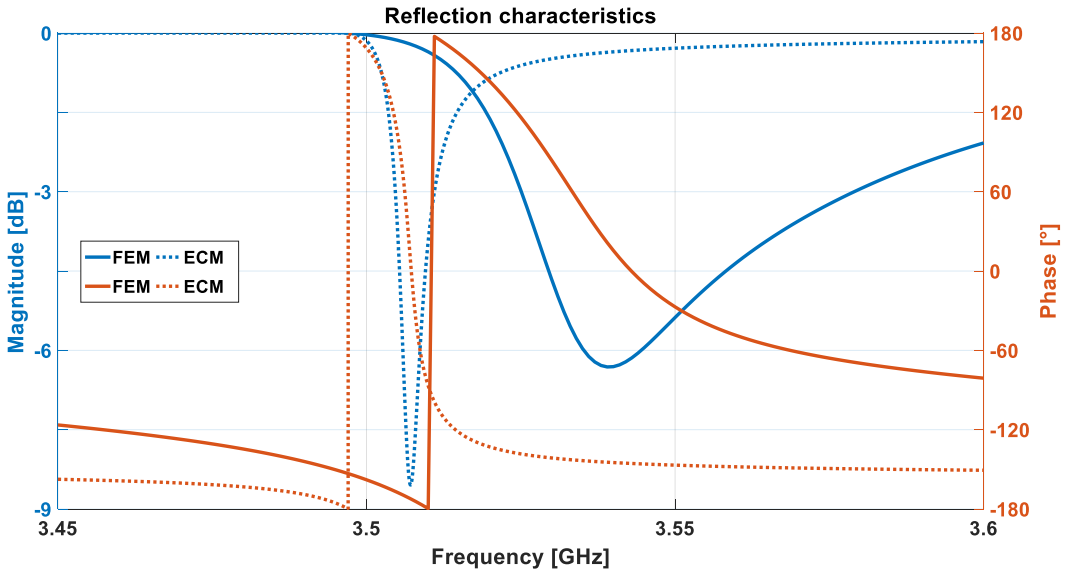

Figure 9: Comparison of the S_{11} curves obtained using COMSOL® (FEM, solid) and the equivalent circuit (ECM, dashed) over [3.45, 3.60] GHz ($f_{01}^{TM} \approx$ 3.50 GHz) in terms of amplitude and phase

To pinpoint the source of error in the ECM that may explain the discrepancies with the finite-element results, a regression method was employed – a least-squares method iteratively attempted to approximate the best combination of parameters (the N_{nm} transformer ratios) needed to recreate the expected results (the full curve of Figure 9). The results of such regression have been compared on Figure 10, in terms of the power-related coefficients $|N_{nm}|^2$ as used in Equation (8), to those calculated by the algorithm that was developed and used to simulate the equivalent circuit (the dashed curve of Figure 9).

One may notice on the left side of Figure 10 that the TM-related transformer ratios that have been calculated are close to those found by the least-squares regression (error of 9%), while the TE-related transformer ratios on the right side of Figure 10 highlight a complete overlook of the N_{41}^{TE} coefficient. Other interesting results on both sides of Figure 10 are that all the modes outside the TM_{0m} and $TE_{4n,m}$ groups have indeed been found not to couple with

the metacell by both methods, as expected by the symmetry considerations. The very nature of the coaxial TE_{41} mode seems therefore to have been neglected and no inductive behavior has been introduced to the ECM by the analytical study. The study led in [9], regarding multi-slit metacells, may provide reason for further investigation. As shown, a metacell composed of many slits may show a total electric field that is slightly more complex than the straightforward sum of the aperture's fields. This would urge one to see the metacell of interest as a multi-aperture, unique cell rather than an assembly of eight independent, mono-slit cells, as implicitly done so far.

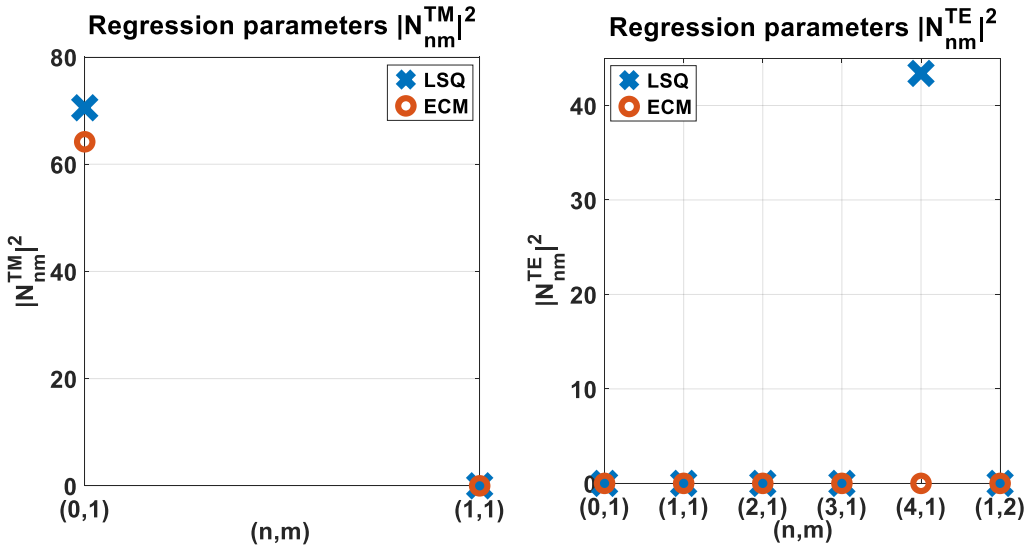

Figure 10: Transformer ratios $|N_{nm}|^2$ as estimated by the least-squares method (LSQ, blue crosses) and calculated by the equivalent circuit model (ECM, red circles)

4 Conclusion

This study aimed at transposing the ECA introduced in [3] to the coaxial geometry of interest, which is a convenient means of emulating free-space propagation at low frequencies. The comparison of the reflection coefficient characteristics highlighted that the ECA applied to the coaxial geometry has indeed been able to account for the resonant behavior, and the mechanisms of the associated mode-conversion, with only a slight frequency shift. However, these same responses also displayed an imperfect adequation of the model concerning the spectral spreading of both the reflection coefficient curves. This error seems to come from an inability of the implemented analytical model to take into account expected couplings of the metacell with some of the TE incident modes, and their inductive contributions, as shown by the regression process.

Yet, the convincing results of [3] warrant further investigation of our metacell: reducing the complex behavior of metasurfaces to simplified, analytical, intelligible equivalent circuit models for design, analysis and integration purposes is key to improving functionality. Besides, the incorporation of electronic lumped elements would also be greatly simplified with equivalent circuits, as demonstrated by [2]. This would pave the way for many further developments, such as providing more appropriate – or at least easier-to-use tools – for the analysis and design of passive and active metasurface systems, interesting for their reconfigurability mechanisms [10] – or even intelligent devices able to self-adapt to external variations [11]. It may also possibly lead to complementary approaches for the analysis and design of space-time modulated metasurfaces, where an electronic point-of-view may be more appropriate as closer to modulation-related schemes, as detailed in [12].

References

[1] S. B. Glybovski, S. A. Tretyakov, P. A. Belov, Y. S. Kivshar and C. R. Simovski, "Metasurfaces: From microwaves to visible," *Physics Reports*, vol. 634, pp. 1-72, 2016.

[2] R. Dubrovka and R. Donnan, "Equivalent circuit of FSS loaded with lumped elements using modal decomposition equivalent circuit method," in *Proceedings of the 5th European Conference on Antennas and Propagation (EUCAP)*, 2011.

[3] F. Mesa, R. Rodriguez-Berral and F. Medina, "Unlocking complexity using the ECA: The equivalent circuit model as an efficient and physically insightful tool for microwave engineering," *IEEE Microwave Magazine*, vol. 19, pp. 44-65, 2018.

[4] L. Brillouin, Wave Propagation in Periodic Structures: Electric Filters and Crystal Lattices, Dover Publications, 2003.

[5] N. Marcuvitz, I. Electrical Engineers, I. Engineering, Technology, M. I. Technology, P. P. Limited, M. I. Technology. Radiation Laboratory, U. S. O. Scientific Research and D. N. D. R. Committee, Waveguide Handbook, McGraw-Hill, 1951, Sections 2.4 & 5.3.

[6] D. E. Horsley, "specialzeros," 2022. [Online]. Available: https://github.com/dehorsley/specialzeros.

[7] C. C. Courtney and E. Donald, "Modes of a double-baffled, cylindrical, coaxial waveguide," 2003. [Online]. Available: http://ece-research.unm.edu/summa/notes/SSN/Note483.pdf. [Accessed August 2021].

[8] D. M. Pozar, Microwave Engineering, 4th Edition, Wiley, 2011, Section 2.3.

[9] R. Rodríguez-Berral, F. Mesa and F. Medina, "Resonant modes of a waveguide iris discontinuity: Interpretation in terms of canonical circuits," *IEEE Transactions on Microwave Theory and Techniques,* vol. 66, pp. 2059-2069, 2018.

[10] Z. Tao, X. Wan, B. C. Pan and T. J. Cui, "Reconfigurable conversions of reflection, transmission, and polarization states using active metasurface," *Applied Physics Letters,* vol. 110, p. 121901, 2017.

[11] B. Chambers and A. Tennant, "A smart radar absorber based on the phase-switched screen," *IEEE Transactions on Antennas and Propagation,* vol. 53, pp. 394-403, 2005.

[12] Z. Wu and A. Grbic, "Serrodyne frequency translation using time-modulated metasurfaces," *IEEE Transactions on Antennas and Propagation,* vol. 68, pp. 1599-1606, 2019.